IOPscience iopscience.iop.org

Home Search Collections Journals About Contact us My IOPscience

Distance-dependent photo-induced electron transport in nanometer-sized junctions

This content has been downloaded from IOPscience. Please scroll down to see the full text.

2016 J. Opt. 18 054004

(http://iopscience.iop.org/2040-8986/18/5/054004)

View the table of contents for this issue, or go to the journal homepage for more

Download details:

IP Address: 169.234.56.87
This content was downloaded on 16/03/2016 at 19:30

Please note that terms and conditions apply.

IOP Publishing Journal of Optics
J. Opt. 18 (2016) 054004 (9pp) doi:10.1088/2040-8978/18/5/054004

Distance-dependent photo-induced electron transport in nanometer-sized junctions

Brian Albee[1], Xuejun Liu[1], Faezeh Tork Ladani[2], Rajen K Dutta[1] and Eric O Potma[1,2]

[1] Department of Chemistry, University of California, Irvine, CA 92697, USA
[2] Department of Electrical Engineering and Computer Science, University of California, Irvine, CA 92697, USA

E-mail: epotma@uci.edu

Received 30 November 2015, revised 11 January 2016
Accepted for publication 22 January 2016
Published 14 March 2016

Abstract

We describe photo-induced current experiments observed in nm-sized electro-migrated nano gaps, using surface plasmon polaritons (SPPs) as the source of the optical driving field. For gaps smaller than 5 nm, we observe a stable photo-induced current that is linear with the intensity of the SPP mode, whereas the photo-current in wider gaps shows a highly nonlinear dependence that is reminiscent of field emission. The results are explained by a modified Wentzel–Kramers–Brillouin tunneling model, which reproduces the observed transition from optical rectification to optically driven field emission in the nano junction.

Keywords: surface plasmon polariton, photo-induced current, nanogap rectenna

(Some figures may appear in colour only in the online journal)

1. Introduction

An optical rectenna is a device that can rectify the modulation of a material's electric polarization at optical frequencies into a dc electron displacement. When such a device is part of a circuit, a dc current may flow [1]. A sub-nm gap between two metal electrodes, such as a metal–insulator–metal (MIM) junction, can act as a rectenna. Not surprisingly, these relatively simple devices have been recognized as potential nano-circuits suitable for converting light to electricity.

In the absence of light, the transport of electrons across sub-nm junctions is conveniently modeled by the Wentzel–Kramers–Brillouin (WKB) approximation for the process of direct tunneling through the potential barrier between the metal electrodes, as described by Simmons [2]. The effective tunneling direction is determined by the asymmetry of gap, typically in the form of a difference between the Fermi levels of the opposing electrodes by applying a bias. For higher electric fields in the junction, the barrier may bend, effectively shortening the tunneling distance and thereby facilitating the transport of electrons across the junction. The latter tunneling mechanism is also known as field emission, as pointed out by Fowler and Nordheim [3, 4].

Upon optical illumination of the gap, the oscillating electric field in the junction sets up a potential difference between the metal electrodes. Classically, the ac optical field produces a dc current in case the gap polarization responds nonlinearly to the modulation [5, 10]. Quantum mechanically, the process of photon-assisted tunneling is commonly described by the model of Tien and Gordon [6, 7], which considers the changes in the electron density of states due to a modulation of the barrier. Photo-induced currents have been observed in a variety of MIM-type junctions. One of the earliest examples of optical rectification was demonstrated in the junction of a scanning tunneling microscope (STM) [8, 9]. Similar observations were made in sub-nm junctions engineered in two-dimensional nano circuits, such as in break junctions [10, 11] or in junctions formed by molecular spacers [12]. In these latter studies, a linear increase in the current is observed as the intensity of the light is raised, consistent with the Tien–Gordon model of optical rectification. For higher gap fields, on the other hand, field emission dominates the tunneling current, as was recently demonstrated in an STM geometry [13].

Although the main properties of a junction-based optical antenna are reproduced by electron tunneling models, many

 © 2016 IOP Publishing Ltd Printed in the UK

questions remain about the details of the tunneling mechanism. In particular, the role of the surface plasmon mode of the junction is not completely understood. For sub-nm junctions, the existence of gap-size dependent charge transfer plasmons has been pointed out, and the importance to include a quantum description of the conduction electrons is very much part of the current debate about the optical properties of gap-nanoantennas [14, 15]. Beyond the challenges in describing the physics of the tunneling process, there are experimental difficulties that limit the complete characterization of sub-nm MIM devices. For instance, fabrication of reproducible MIM junctions in the (sub-)nm regime remains a difficult task. In addition, heating effects upon illumination can comprise the stability of the junction. Morphological changes on the Ångström scale can affect the optical properties of the device and thus significantly alter the photo-induced tunneling current.

In this work, we focus on MIM gap-antennas in the nm range (4–20 nm), a regime for which quantum effects of the plasmonic response are deemed unimportant. We find that gaps in this range are reproducibly fabricated with electromigration methods. Using a remote excitation scheme based on propagating surface plasmon polaritions (SPPs) for driving the surface plasmon mode in the gap, we observe a stable performance of the optical rectennas under ambient conditions. The stability of the devices makes it possible to study their photo-induced currents in detail. Our studies indicate that for narrower gaps, a transition between Tien–Gordon type tunneling and Fowler–Nordheim field emission can be observed, while in wider gaps field emission is the dominant mechanism for electron transport across the nano junction.

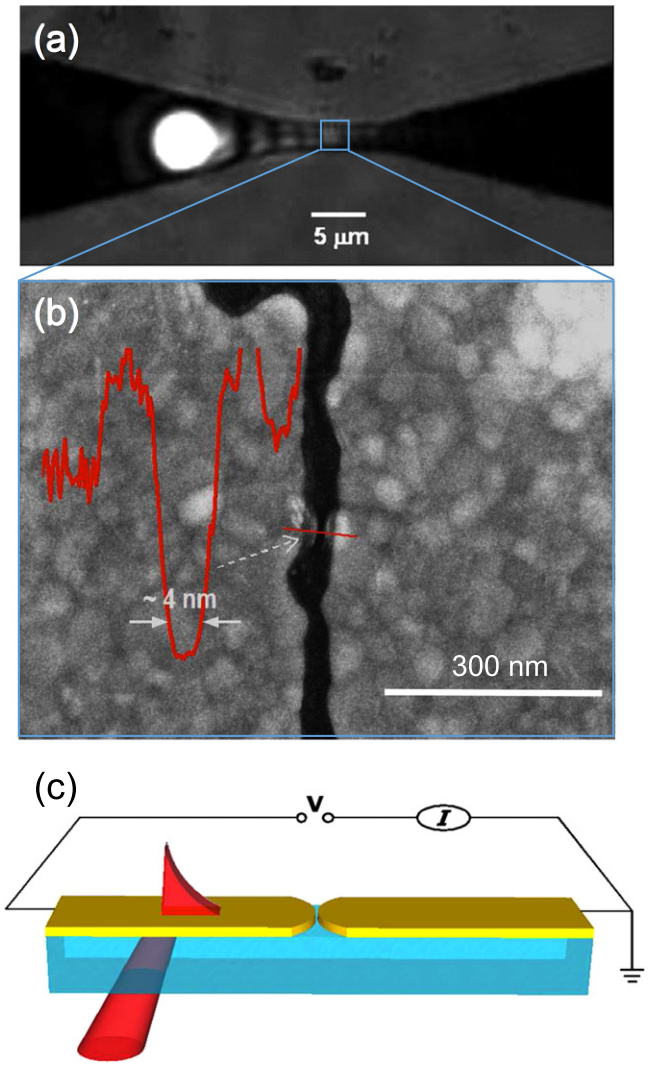

Figure 1. Experimental layout. (a) Optical transmission image of two tapered electrodes. (b) SEM image of the slit junction between the electrodes. The shortest distance is formed by an electromigrated protrusion. (c) Schematic of the photo-induced current measurement. The laser beam is incident at the Kretschmann angle to launch a SPP mode at a distance of ~10 μm away from the junction.

2. Materials and methods

2.1. Sample fabrication

Tapered gold electrodes were fabricated by a photolithography procedure combined with electromigration, adapted from [16–19]. Thin borosilicate cover slips (Fisher Scientific) were cleaned in reactive oxygen plasma (Harrick Plasma). A 20 nm Au film was deposited onto the glass after application of a 1 nm Cr adhesion layer. A positive polymer resist (Dow, S1808) was spun onto the films, after which the slides were baked at 90 °C for 30 min. A chrome mask was used for UV-based photolithography, using an exposure time of 1.25 s. The exposed slides were developed in MF-319 and etched in Gold Etchant TFA (Transene Company) to yield the final Au patterned films. This procedure consistently produced two tapered electrodes connected by a channel with a length of a ~5 μm and a width of ~2 μm, as shown in the transmission image of figure 1(a).

Nanometer-sized junctions were prepared in the channel by using a combination of focused ion beam (FIB) milling (FEI Quanta 3D FEG) and electromigration. First, using FIB milling, the width of the central portion of the channel was reduced to ~500 nm. A partial cut was prepared across the width of the channel, yielding a ~20 nm wide cleft. This intentionally incomplete milling procedure gave rise to several intact Au grains in the cleft, forming a conducting junction. The sample was cleaned and treated with ceric ammonium nitrate-based chromium etchant (Sigma Aldrich) to remove remaining chromium in the junction. The sample was then electro-migrated, and exposed to a final chromium etchant treatment (Transene Company). The fabricated nano junctions were characterized with a high-resolution SEM (FEI Magellan 400L) to verify the size of the electro-migrated gap introduced into the sample at a resolution of 0.9 nm. This procedure consistently yielded nanojunctions between 4–12 nm under ambient conditions. Figure 1(b) shows an SEM micrograph of a junction. The indicated electro-migrated grain displays a gap width of ~4 nm.

2.2. Experimental layout

The experiments were conducted in an optical microscope (IX71, Olympus). The excitation beam was derived from a 76 MHz Ti:sapphire laser (Mira 900, Coherent), which produces pulses with a center wavelength of 800 nm and a temporal width of 250 fs at the sample plane. Part of the laser beam was used to drive a home-built, synchronously pumped optical parametric oscillator, which delivered tunable 200 fs pulses between 950 and 1200 nm. The polarization orientation of the incident laser beam was controlled with an achromatic half-wave plate. The excitation beam is passed through a 1.0 mm pinhole near the back aperture of a high numerical aperture lens (60x, NA 1.42 oil, Olympus) and focused loosely onto the Au film. The pinhole was placed such that the pencil beam was incident on the sample at the Kretchmann angle for exciting a SPP mode at the gold/air interface. The diameter of the focal spot at the Au film was $\sim 3\ \mu$m and the distance between the SPP launching site to the nanogap was $\sim 10\ \mu$m. The remote launching spot of the SPP mode and its subsequent propagation to the nano junction was monitored by imaging the leakage radiation onto an EMCCD camera (iXon3, Andor) [20]. For four-wave mixing (FWM) and two-photon excited luminescence (TPEL) measurements, a dichroic mirror (680 SWP, Chroma) was inserted to separate the back-scattered nonlinear optical signals from the incident laser light [22]. Figure 1(c) shows a sketch of the excitation configuration.

A Keithley 2400 sourcemeter was used to control the bias across the nano junction. To measure the photo-induced current across the junction, the laser light was amplitude modulated at 200 Hz. The current measured in the circuit was amplified with a pre-amplifier (Model 1211, DL Instruments) and detected with a lock-in amplifier (SR830, Stanford Research Systems). The demodulated output was fed into a computer for registering the signal. The sensitivity of the current measurements was 0.02 pA, which constitutes the noise floor. For current measurements as a function of laser power, a laser power controller (Brockton Electro-Optics) was used to control the average laser power. Typical average powers at the sample plane were in the 0.1–1 mW range. A script was written to carry out rapid sweeps of the laser power while monitoring the current through the junction.

2.3. Full wave simulations

An estimation of the electric field amplitudes in the nano junction was obtained from three-dimensional finite element method (FEM) full wave simulations, carried out with COMSOL 4.4 using the wave optics module. The device was modeled as a 30 nm thick gold layer on glass. The size and shape of the device was chosen according to the experimental parameters given in section 2.1. A variable mesh was used, with the smallest mesh size of ~ 2 nm at the nanogap and larger mesh sizes away from the junction. The excitation was modeled as a Gaussian beam with a focal radius of 1.0 μm, incident at the Kretschmann angle.

3. Results

3.1. SPP-based excitation of gap mode

In this work, we have chosen to drive the gap mode through SPP-based excitation. In this configuration, an SPP mode is launched $\sim 10\ \mu$m away from the nanogap and allowed to propagate to the junction. Based on a three-dimensional model for the asperities in the slit [17], we have simulated the propagation of SPP waves near the junction using FEM simulations. Upon traversing the nanometer-sized slit between the electrodes, part of the energy contained in the SPP mode couples to asperities in the the gap [21], as shown in figure 2. The excitation of local gap modes produces enhanced local fields, F_{opt}, which are generally strongest at the narrower gaps [17]. A rough estimation of the strength of F_{opt} can be obtained from the FEM simulation. We find that pulsed local fields for a 4 nm gap on the order of 0.1–1.0 V nm^{-1} are feasible using the experimental excitation conditions examined here. Similar values have been reported for metal–insulator–metal junctions under comparable experimental illumination conditions [10, 13]. Such optical gap fields have previously shown to enable the generation of photo-induced currents.

3.2. SPP-induced currents

To investigate whether the gap modes excited by the SPP waves can generate a photo-induced current, we have first examined the current as a function of the polarization orientation of the incident laser light. For these measurements, junctions with 4 nm gaps were used and the average laser power density was set to 24 kW cm^{-2} (1.3×10^9 W cm^{-2} peak power density) at 800 nm, while a 0.2 V dc bias was applied across the junction. Upon illumination of the electrode, pA-level currents were measured in the circuit. Figure 3(a) shows the measured current as a function of the polarization angle θ. A maximum current is obtained when the beam is *p*-polarized relative to the gold surface ($\theta = 90°$). The current decreased as the polarization was changed and reached the noise level when the beam was *s*-polarized. Fitting the signal to the function $\sin^2\theta$ yielded excellent agreement. These observations strongly suggest that the observed current is induced by the SPP mode. In addition, the polarization dependence indicates that the photo-induced current, in this regime, is linearly dependent on the incident power of *p*-polarized light. We also note that in the absence of light, the measured current reaches the noise floor (<0.1 pA), indicating that at the biases examined here (0–0.6 V), no background current was observed.

These results suggest the process of optical rectification in nanometer-sized junctions. To investigate whether the observed current can be classified as a rectified current, we excited the junction with two SPP modes. To accomplish this, two laser beams with wavelengths of 800 and 1040 nm, respectively, were incident on the gold electrode simultaneously. Each of the SPP modes gave independently rise to a photo-induced current in the nano gap circuit. When the SPP

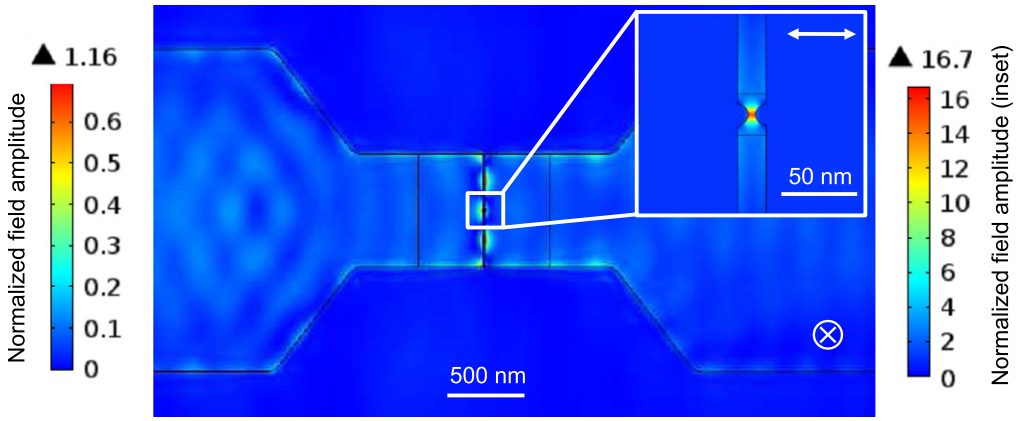

Figure 2. FEM simulation of propagating SPP waves in the vicinity of the junction, using an excitation wavelength of 800 nm and a film thickness of 30 nm. The scale bar on the left shows the magnitude of the field in normalized units relative to the magnitude of the incident light field. The SPP propagation is from left to right. The out of plane electric field component is shown. The inset shows the nanogap, formed by protrusions in the slit junction, where the electric field component polarized longitudinally in the gap is highly concentrated. The scale bar to the right shows the magnitude of the field depicted in the inset, normalized to the amplitude of the incident field. In this simulation, the effective enhancement in the nanogap relative the initial electric field is ~16.

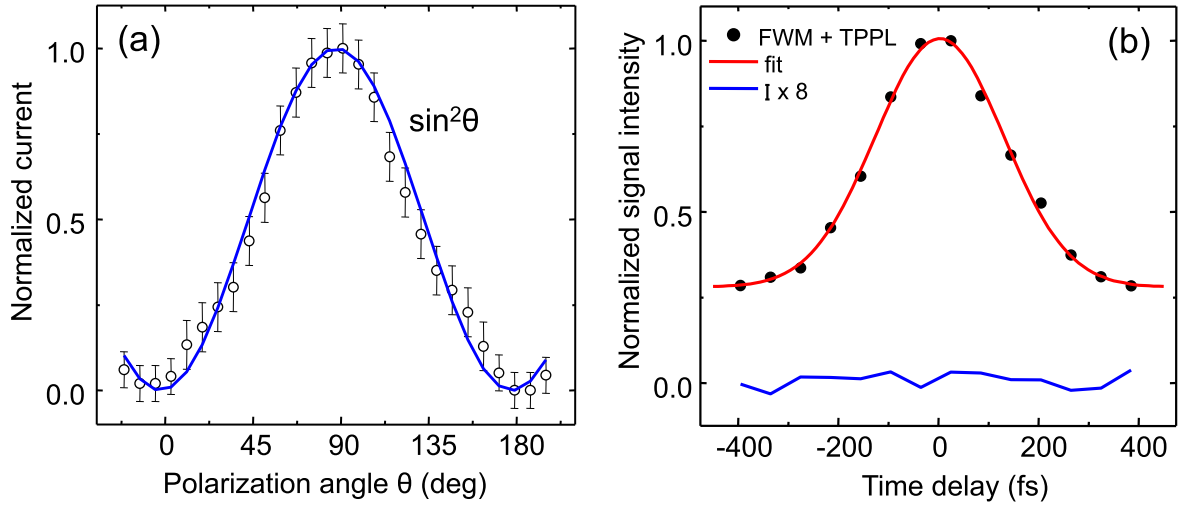

Figure 3. Polarization dependence of induced tunneling current under an incident laser power density of 24 kW cm^{-2} (800 nm) and a bias of +0.2 V. The current is normalized to the highest value in the measurement. (b) Time scan results of the nonlinear optical signal (FWM and TEPL) generated from the 4 nm gap and simultaneously collected gap tunneling current (blue curve) using a bias of +0.2 V and incident laser powers of 24 kW cm^{-2} (800 nm beam) and 32 kW cm^{-2} (1040 nm beam).

pulses were temporally offset, the total current was the sum of their individual contributions. Upon overlapping the SPP pulses temporally, as verified by the FWM and the TPEL emission of the gap mode (figure 3(b)), no additional current contributions were observed. The experiment was repeated by amplitude modulating each beam at a different frequency (200 Hz and 240 Hz, respectively), while detecting the current at the difference frequency (40 Hz). Under all conditions examined, no increase in the current was observed when the SPP pulses were temporally overlapped. These results indicate that the dc electron current is not driven by a nonlinear process that involves two independent fields with optical frequencies ω_1 and ω_2, where $\omega_1 \neq \omega_2$. This notion is consistent with a coherent optical rectification process, which does not produce a dc current when $\omega_1 - \omega_2 \neq 0$. An incoherent process, whereby the electron is first photo-excited to a (dephased) hot electron state by a first pulse, and subsequently excited to a higher lying state by the second pulse, followed by tunneling of the doubly excited electron ($\hbar\omega_1 + \hbar\omega_2$), is also incompatible with these observations. Therefore, we conclude that the observed dc current originates from a coherent rectification process.

3.3. Gap-size dependent electron transport

We next studied the photo-induced current as a function of the magnitude of the optical field in the junction. The subsequent results were obtained for *p*-polarized incident fields. Figure 4(a) shows the current for different average powers of the incident 800 nm laser beam, obtained while maintaining a dc bias of 0.6 V. The current is shown as a function of F_{inc}, the amplitude of the incident field at the launching site,

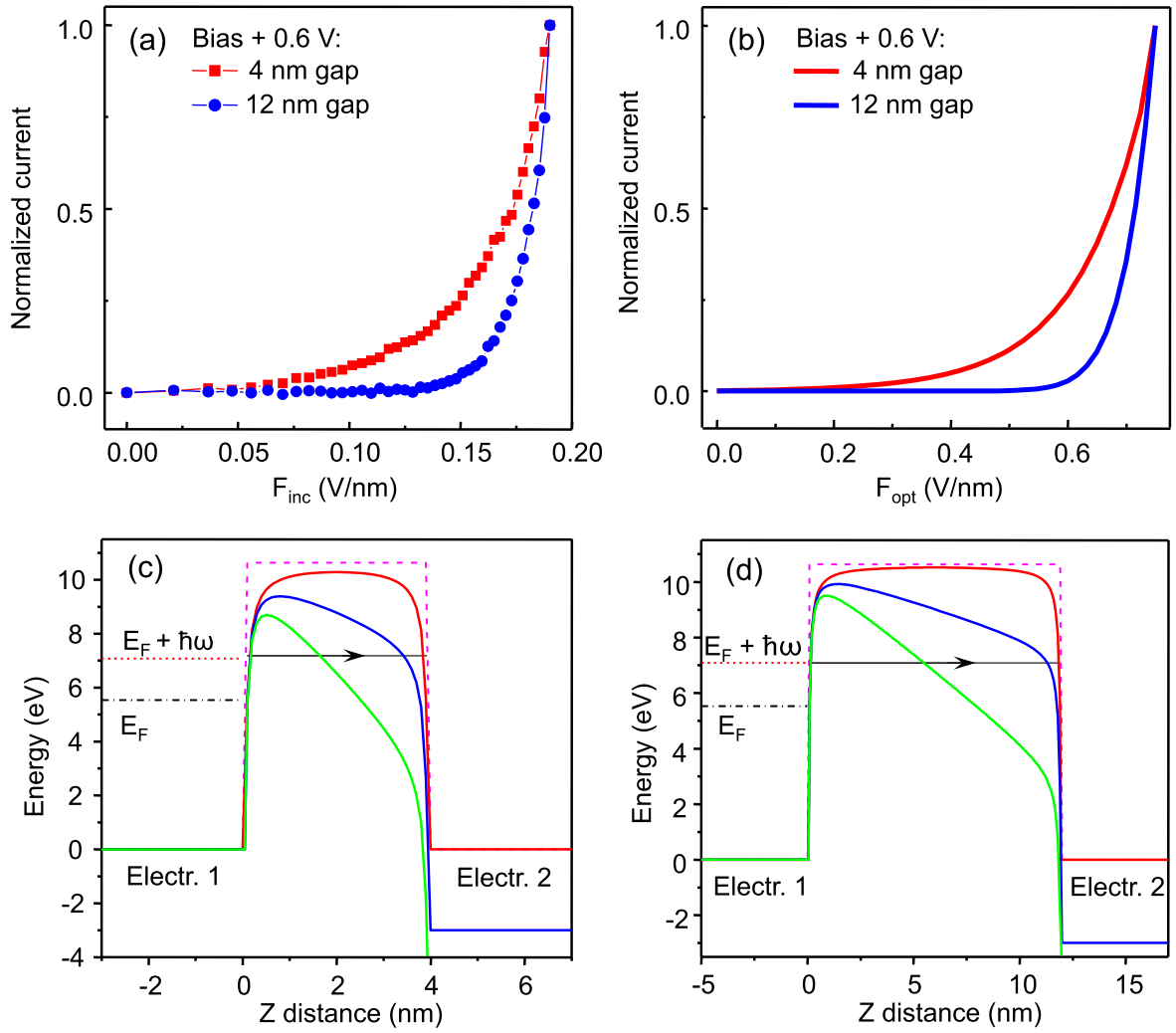

Figure 4. (a) Tunneling current as a function of incident laser peak field amplitude F_{inc} of two nanogaps with different gap sizes. The current is normalized to the highest value in the measurement. (b) Calculated tunneling current as a function of assumed local gap field intensity for two similar nanogaps. (c) and (d) The original rectangular barrier and barriers with the image potential included under different biases of our MIM nanojunction structure for the 4 and 12 nm nanogaps respectively. In both figures, the black dashed–dotted line and the red dotted line correspond to the Fermi energy and to an excited state at (E_F + 1.55 eV). The biases are 0 V (red), 3 V (blue) and 7.5 V (green).

determined from the peak power of the optical pulse. The red curve corresponds to the current measured in a 4 nm junction, whereas the blue curve was obtained from a 12 nm junction. In both measurements, a low current is observed at lower illumination doses, which rapidly increases for higher intensities of the optical field in the junction. In the narrower junction, however, the current displays a more gradual increase at lower incident powers, showing a quasi-linear dependence, which is not seen for the wider junction. Compared to the 4 nm junction, the magnitude of the photo-induced current in the 12 nm gap shows a steeper dependence on the incident light when the laser power is raised. The difference between the laser intensity dependence of narrow (<5 nm) and wide (>10 nm) junctions is reproducible, indicating that the mechanism that underlies the rectification process is gap-size dependent.

In order to gain insight in the photo-induced electron transport across the junction, we modeled the current with a simple model based on the WKB approximation to the electron tunneling probability across a MIM junction. Within this approximation, the tunneling probability D can be written as:

$$D(E_z) = \exp\left[-\frac{2\sqrt{2m}}{\hbar}\int_{z_1}^{z_2}\sqrt{V(z) - E_z}\,\mathrm{d}z\right], \qquad (1)$$

where m is the mass of the electron, $V(z)$ is the barrier potential and E_z is the energy of the electrons involved in the tunneling process along the z-coordinate. In the presence of a dc bias of V_b, the tunneling current density J can be formulated as:

$$J(V_b) = \int_0^{E_{\mathrm{m}}} D(E_z)\zeta(E_z, V_b)\mathrm{d}E_z \qquad (2)$$

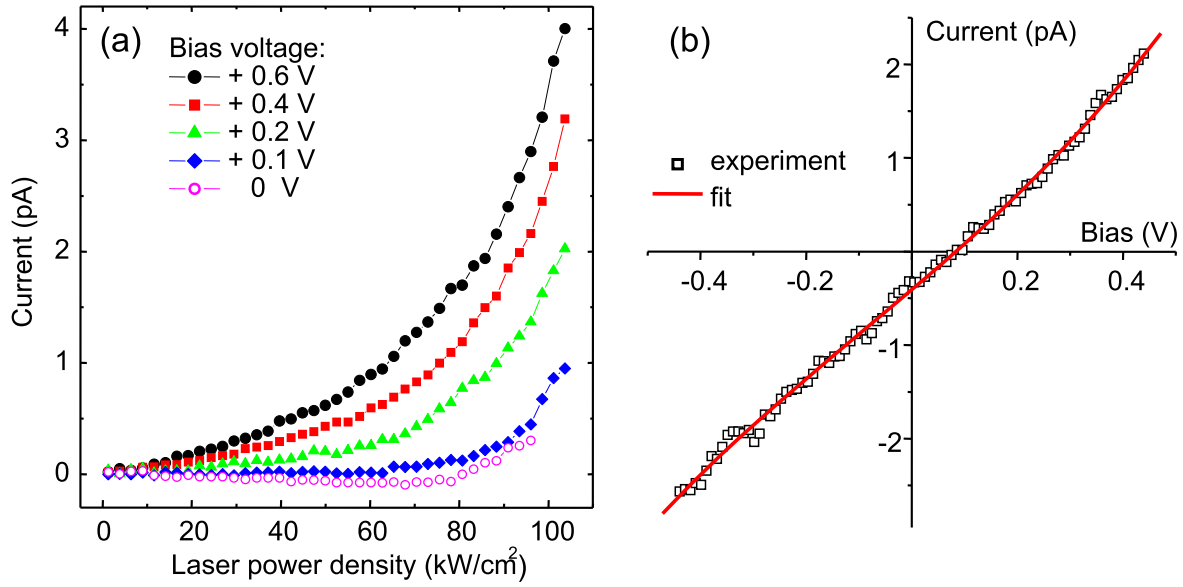

Figure 5. (a) Tunneling current as a function of the average laser power density at the launching site under different bias voltages for a device with a 4 nm nanogap. (b) *I–V* curve obtained with an average laser power density of 90 kW cm^{-2} for a device with a 4 nm nanogap. The polynomial fit (red curve) serves here as a guide to the eye.

with E_{m} the maximum energy of the tunneling electrons and $\zeta(E_z, V_b)$ given as [2]:

$$\zeta(E_z, V_b) = \frac{4\pi me}{h^3}\int_0^{\infty}[f_1(E_z + E_r) - f_2(E_z + E_r + eV_b)]\mathrm{d}E_r. \quad (3)$$

Here $f(E)$ is the Fermi–Dirac distribution function. The integration in equation (3) is over the electron energies of the lateral degrees of freedom ($r = \{x, y\}$). We used equation (2) to simulate the current in 4 and 12 nm sized junctions. The simulations assumed a Fermi energy of 5.53 eV and work function of 5.1 eV for Au. The photon energy of the incident laser was 1.55 eV and the optical field was allowed to modulate the barrier. The tunneling current is obtained after integrating over one optical cycle of the driving field. The nonlinearity of the gap junction is modeled by assuming an asymmetry in the optically modulated gap polarization, whereby the effective gap field $F_{\mathrm{opt}}\sin\omega t$ during one half of the optical cycle exhibits a slightly higher amplitude than the other half of the optical cycle, i.e. $F_{\mathrm{opt}}(t < T_{1/2}) > F_{\mathrm{opt}}(t > T_{1/2})$ with $T_{1/2}$ the half-cycle time. In addition, we included the image potential to describe the potential barrier $V(z)$ [2]. In the simulations, we have assumed that electrons driven at energies $E_F + \hbar\omega$ are the primary tunneling electrons.

The simulated tunneling current is a sensitive function of the applied bias, magnitude of the optical field, and the width of the gap. Figure 4(b) shows a simulation of the current as a function of the gap field F_{opt}. The asymmetry of the gap polarization affects the magnitude of the photon-induced current, but does not significantly change the profile of the simulated curve. The laser power dependence of the photo-induced current depends primarily on the magnitude of F_{opt} and the gap width. The simulated range of the field strength corroborates our estimates based on FEM simulations. For the examined field strengths (~0.1 V nm^{-1} range), we found consistently different current-versus-intensity profiles for the 4 and 12 nm junctions in the simulations, which closely mimic the experimentally observed curves. The strong agreement between the simulation and the measurements suggests that a simple tunneling model in the presence of optical modulation is sufficient to explain the observed differences between the junctions.

Figures 4(c) and (d) show the tunneling barrier for the 4 and the 12 nm junction, respectively. The bending of the barrier potential is indicated for various values of the potential difference across the gap, which is a sum of the applied dc bias and the potential introduced by the ac modulation of the optical field. The tunneling electron at $E_F + \hbar\omega$ is indicated by the arrow. We note that when the energy of the tunneling electron is set at E_F, qualitatively comparable current-versus-intensity profiles as in figure 4(b) are observed by adjusting the simulated range of F_{opt}. This indicates that the model cannot conclusively determine the energy of the electrons that are transported across the junction. Hence, the simulation cannot unambiguously discriminate between Fermi-level electrons or photo-excited electrons as the primary tunneling charges.

Figure 5(a) shows the laser power dependence of the current for different values of V_b for a device with a 4 nm gap. Under all conditions, we observe a quasi linear dependence of the photo-induced currents at lower illumination levels, whereas a strongly nonlinear dependence is seen at higher illumination doses. In this device, for $V_b < 0.1$ V, the current is negative below 60 kW cm^{-2}. Figure 5(b) depicts the *I–V* curve for a different device with a nanogap of ~4 nm when the laser power is set to 90 kW cm^{-2}. For this junction, a

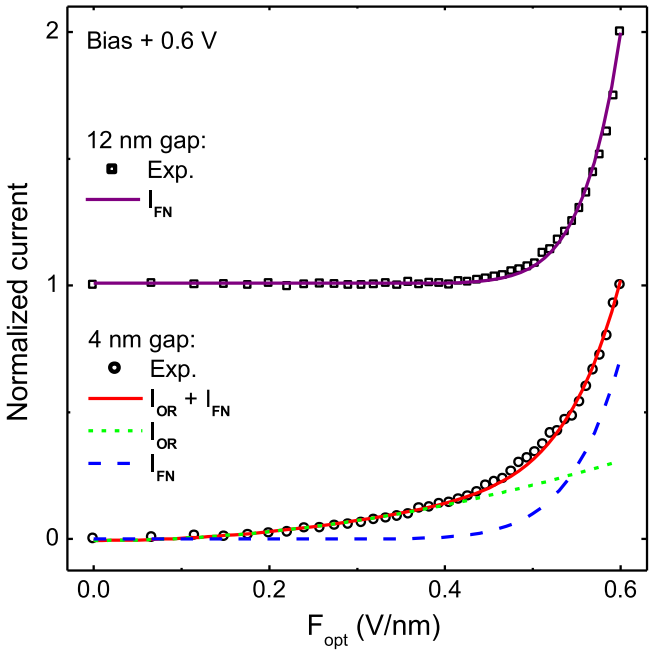

Figure 6. Photo-induced current in two devices with different gap width as a function of laser illumination levels. Top curve shows the results for the 12 nm gap and the lower curve shows the results for the 4 nm gap. Experimental points are indicated by open black dots. Fits are represented by solid lines. The purple line is a fit using I_{FN} (equation (5)) using a Fowler–Nordheim coefficient of $c = 8.4$ V nm^{-1}. The red line is a fit based on $I_{FN} + I_{OR}$ using $c = 8.2$ V nm^{-1}, with the I_{OR} contribution indicated by the green dashed line, and the I_{FN} contribution by the blue dashed line. Experimental curves are off-set for clarity.

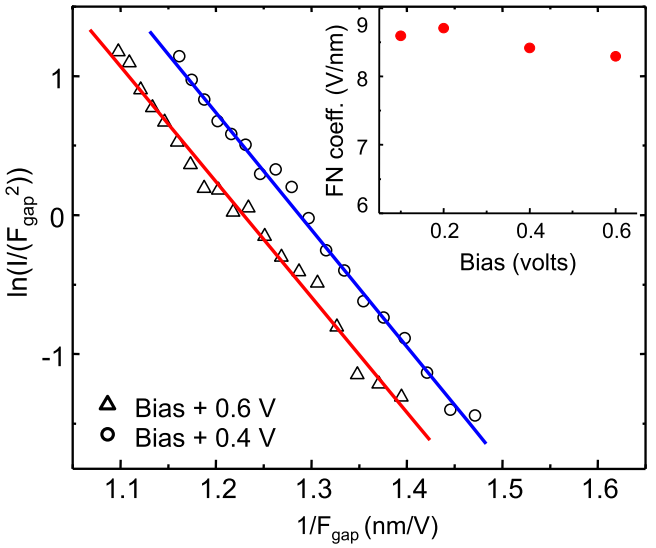

Figure 7. Fowler–Nordheim fit to the photo-induced current in the nonlinear regime for the 4 nm gap measured at various settings of V_b. The inset shows the Fowler–Nordheim (c) coefficient obtained from the fit for measurements at different biases.

negative current is produced at $V_b = 0$, driven solely by the photo-induced electron transport process.

3.4. Linear versus nonlinear power dependence of photo-induced current

Although the experimental data is satisfactorily reproduced with the WKB model plus optical modulation, this description does not explicitly discriminate between the established mechanisms of Tien–Gordon type rectification and Fowler–Nordheim field emission; two mechanisms with very distinct dependences of the current on the strength of the gap field. Classical and quantum models for the process of optical rectification designate a linear dependence of the current with the intensity of the optical field F_{opt}[10]:

$$I_{OR} = I_0 + aF_{opt}^2, \tag{4}$$

where a is a constant that is proportional to the second order nonlinearity $(\partial^2 I/\partial V^2)_0$ of the junction [10]. The current in the absence of the optical field is indicated as I_0. Field emission as predicted by Fowler–Nordheim yields a dc current that scales as [3, 23]:

$$I_{FN} = bF_{gap}^2 \exp\left[-\frac{c}{F_{gap}}\right], \tag{5}$$

where $b = e^3\lambda/(8\pi h\phi)^{-1}$ and $c = \alpha\phi^{3/2}$, with λ a correction factor, ϕ the work function and α a constant with units (eV$^{3/2}$ nm V^{-1}). Here $F_{gap} = F_b + F_{opt}$, where F_b is the applied bias field. Equation (5) is valid for a triangular barrier into vacuum, and, as such, shows no explicit dependence on the width of the junction. The profile obtained for the 12 nm junction can be fitted well with equation (5), reproducing the steep exponential rise of the current as the laser power is increased shown in the top curve of figure 6. For this larger gap size, the tunneling process thus shows similarities to pure field emission through a bent barrier, which is irrespective of the width of the junction. Indeed, we have found a similar dependence for the photo-induced current across wider gaps in the 12–20 nm range, all of which can be fitted to the Fowler–Nordheim type function of equation (5).

The profile for the 4 nm junction, however, cannot be mapped onto a profile predicted by equation (5). For lower laser power densities (<60 kW cm^{-2}), the current shows a quasi-linear dependence which is not reproduced with the Fowler–Nordheim expression, but is instead reminiscent of the linear dependence predicted by Tien–Gordon type optical rectification as in equation (4).

For higher laser power densities (>60 kW cm^{-2} average, 3.2×10^9 W cm^{-2} peak), the conductance of the 4 nm junction grows more nonlinear and the current approaches a profile that mimics the Fowler–Nordheim power dependence of equation (5). The complete power dependence of the photo-induced current measured in the 4 nm junction can be phenomenologically fitted to a function that is a combination of equation (4) and equation (5), i.e. $I = I_{OR} + I_{FN}$. The lower curve in figure 6 includes a fit to the current as a function of laser power based on this composite function. It can be seen that at low power a quasi-linear dependence is evident while at higher field intensities in the junction the exponential dependence gains prominence. Note that this

behavior was consistently observed for a wide range of biases (0.1–0.6 V).

To examine the nature of the current for higher intensities of the optical field, we subtracted the linear dependence and plotted $\ln\left[I/F_{\mathrm{gap}}^{2}\right]$ as a function of F_{gap}^{-1}, for several settings of the bias V_b. The results are shown in figure 7. The logarithmic dependence observed confirms that the photo-induced current follows a Fowler–Nordheim type dependence, where the slope of the profile corresponds to the c coefficient in equation (5). The extracted c coefficient is given for various values of the V_b in the inset of figure 7. This observation indicates that Fowler–Nordheim tunneling provides a good description in the high power regime for all settings of the bias examined here. We find a Fowler–Nordheim c coefficient that averages to $\sim$8.6 V nm^{-1} across the measurements, close to a previously reported value for Fowler–Nordheim tunneling [13]. The variation in c is small throughout various measurements, which confirms the repeatability of the photo-induced current measurements. The fact that the junction conductance was not quantitatively altered during the experiments provides strong evidence that the morphological integrity was preserved during the measurements.

4. Discussion

In this work, we have fabricated nanometer-sized junctions and investigated their rectifying properties under optical illumination. We have adopted a remote excitation scheme, where an SPP field is launched away from the junction, thus avoiding direct illumination of the junction with freely propagating light. Instead, the junction plasmon is excited by the SPP field. We have found that this arrangement allows stable generation of photo-induced currents, even at ambient temperatures and pressures. Our experiments show that the SPP mode is responsible for excitation of the gap mode, as evidenced by a clear polarization dependence of the photo-induced current. The remote excitation scheme presented here appears to have favorable heat dissipation dynamics, which reduces local heating of the junction and limits photo-induced morphological changes of the gap. The robustness of this approach is reflected in the stability of the Fowler–Nordheim c coefficient, which remained unaltered during our experiments.

We have observed stable photo-induced currents in junctions of variable gap widths. The dependence of the current as a function of laser power was found to be consistently different for narrow gaps (<5 nm) versus wider gaps (>10 nm). Whereas wider gaps show a characteristic exponential dependence, which can be explained by assuming a Fowler–Nordheim field emission process, narrower gaps show an additional linear component that is reminiscent of an optical rectification process previously observed in sub-nm gaps. In the 4 nm junction examined here in detail, we have found a transition between the linear optical rectification process at lower intensities of the optical field to an exponential field emission process at higher intensities.

Optical rectification is usually associated with sub-nm junctions, where direct tunneling of the electron through the barrier can be observed even at low intensities of the optical field. However, our experiments suggest that this principle can be extended to nm-sized gaps. Although direct tunneling probabilities are negligible in nm gaps, strong gap fields can modulate the barrier sufficiently as to allow electrons to penetrate the distorted barrier. This process produces a linear dependence of the current on the field intensity. At even stronger fields, the barrier bends, and clear Fowler–Nordheim tunneling becomes more prominent. A similar transition from optical rectification to field emission of electrons across the gap has previously been observed in sub-nm metal–molecule–metal junctions [24] and in STM tunneling junctions [13].

Although optical rectification and field emission are commonly considered distinct tunneling mechanisms, a numerical simulation based on a simple WKB model reproduces all the observed trends in our experiments, including the transition from a linear to a nonlinear (exponential) dependence. Both regimes follow naturally from the optical modulation of the gap barrier, which allows tunneling of the electrons through the thinning of the barrier. Using WKB tunneling combined with optical modulation, the linear regime is retrieved only for the narrower gap, whereas the wider gap displays solely Fowler–Nordheim type tunneling under the conditions examined here. The model also predicts that for higher gap fields, the tunneling mechanism in both the narrow and wide gaps resembles the process of field emission.

These observations suggest that, for the the nm-sized gaps studied here, the same physical mechanisms underlie the generation of photo-induced currents in the linear and nonlinear regimes. Both the linear and nonlinear regime produce rectified currents, and both regimes appear to follow from a tunneling process in which the resulting current is coherently rectified by the optical field. The simple WKB model used here cannot conclusively identify the energy of the tunneling electrons, as qualitatively similar results are obtained for tunneling electrons of energies E_F or $E_F + \hbar\omega$. Previous tunneling studies have suggested that photo-excited electrons, which have lost their coherence relative to the driving field after dephasing, are the primary tunneling charges in the junction [25]. Although our measurements do not exclude the involvement of dephased electrons, our two-color photo-induced current experiment suggests that contributions from incoherent, nonlinearly excited electrons are negligible.

5. Conclusion

This study shows that stable and reproducible photo-induced currents can be generated in nm-sized gaps under ambient conditions, using propagating SPP modes to drive the gap fields. The resulting current shows contributions from direct

optical rectification and from field emission, where the relative weight of these processes shows a dependence on the width of the gap. These observations can be explained with a simple WKB model supplemented with optical modulation, which reproduces the transition between linear to nonlinear photo-induced currents. The stability of the gap antennas in the nm regime under benign SPP excitation conditions underlines their promise as rectennas for light to energy conversion.

Acknowledgments

We thank Ara Apkarian for useful discussions. This work was supported by the Department of Energy, grant DE-SC0003905. XL and FTL are grateful for support of the National Science Foundation, Center for Chemical Innovation, Grant CHE-1414466. SEM and FIB work was performed at the UC Irvine Materials Research Institute (IMRI).

References

[1] Corkish R, Green M A and Puzzer T 2002 Solar energy collection by antennas *Sol. Energy* **73** 395–401
[2] Simmons J G 1963 Generalized formula for the electric tunnel effect between similar electrodes separated by a thin insulating film *J. Appl. Phys.* **34** 1793–803
[3] Fowler R H and Nordheim L 1928 Electron emission in intense electric fields *Proc. R. Soc.* A **19** 173–81
[4] Gadzuk J W and Plummer E W 1973 Field emission energy distribution (FEED) *Rev. Mod. Phys.* **45** 487–548
[5] Tu X W, Lee J H and Ho W 2006 Atomic-scale rectification at microwave frequency *J. Chem. Phys.* **124** 021105
[6] Tien P K and Gordon J P 1963 Multiphoton process observed in the interaction of microwave fields with the tunneling between superconductor films *Phys. Rev.* **129** 647–51
[7] Tucker J R 1979 Quantum limited detection in tunnel junction mixers *IEEE J. Quantum Electron.* **15** 1234–58
[8] Lucas A A, Cutler P H, Feuchtwang T E, Tsong T T, Sullivan T E, Yuk Y, Nguyen H and Silverman P J 1988 Use of a scanning tunneling microscope to rectify optical frequencies and measure an operational tunneling time *J. Vac. Sci. Technol.* A **6** 461–5
[9] Bragas A V, Landi S M and Martínez O E 1998 Laser field enhancement at the scanning tunnelling microscope junction measured by optical rectification *Appl. Phys. Lett.* **72** 2075–7
[10] Ward D R, Hüser F, Pauly F, Cuevas J C and Natelson D 2010 Optical rectification and field enhancement in a plasmonic nanogap *Nat. Biotechnol.* **5** 732–6
[11] Stolz A, Berthelot J, Mennemanteuil M M, Colas de Francs G, Markey L, Meunier V and Bouhelier A 2014 Nonlinear photo-assisted tunneling transport in optical gap antennas *Nano Lett.* **15** 2330–8
[12] Arielly R, Ofarim A, Noy G and Selzer Y 2011 Accurate determination of plasmonic fields in molecular junctions by current rectification at optical frequencies *Nano Lett.* **11** 2968–72
[13] Dey S, Mirell D, Perez A R, Lee J and Apkarian V A 2013 *J. Chem. Phys.* **138** 154202
[14] Esteban R, Zugurramuri A, Zhang P, Nordlander P, García-Vidal F J, Borisov A G and Aizpurua J 2015 A classical treatment of optical tunneling in plasmonic gaps: extending the quantum corrected model to practical situations *Faraday Disc.* **178** 151–83
[15] Wu L, Duan H, Bai P, Bosman M, Yang J K W and Li E 2013 Fowler–Nordheim tunneling induced charge transfer plasmons between nearly touching nanoparticles *ACS Nano* **7** 707–16
[16] Ward D R, Grady N K, Levin C S, Halas N J, Wu Y, Nordlander P and Natelson D 2007 Electromigrated nanoscale gaps for surface-enhanced Raman spectroscopy *Nano Lett.* **8** 1396–400
[17] Ward D R, Halas N J, Ciszek J W, Tour J M, Wu Y, Nordlander P and Natelson D 2008 Simultaneous measurements of electronic conduction and Raman response in molecular junctions *Nano Lett.* **8** 919–24
[18] Xiang C, Kim J Y and Penner R M 2009 Reconnectable sub-5 nm nanogaps in ultralong gold nanowires *Nano Lett.* **9** 2133–8
[19] Xing W, Hu J, Kung S C, Donovan K C, Yan W, Wu R and Penner R M 2012 A chemically-responsive nano junction within a silver nanowire *Nano Lett.* **12** 1729–35
[20] Hecht B, Bielefeldt H, Novotny L, Inouye Y and Pohl D W 1996 Local excitation, scattering, and interference of surface plasmons *Phys. Rev. Lett.* **77** 1889–92
[21] Zhang L, Kubo A, Wang L, Petek H and Seideman T 2013 universal aspects of ultrafast optical pulse scattering by a nanoscale asperity *J. Phys. Chem.* C **117** 18648–52
[22] Liu X, Wang Y and Potma E O 2011 Surface-mediated four-wave mixing of nanostructures with counterpropagating surface plasmon polaritons *Opt. Lett.* **36** 2348–50
[23] Forbes R G 2008 Physics of generalized Fowler–Nordheim-type equations *J. Vac. Sci. Technol.* B **26** 788–93
[24] Beebe J M, Kim B, Gadzuk J W, Frisbie C D and Kushmerick J G 2006 Transition from direct tunneling to field emission in metal–molecule–metal junctions *Phys. Rev. Lett.* **97** 026801
[25] Pal P P, Jiang N, Sonntag M D, Chiang N, Foley E T, Hersam M C, Van Duyne R P and Seideman T 2015 Plasmon-mediated electron transport in tip-enhanced Raman spectroscopic junctions *J. Phys. Chem. Lett.* **6** 4210–8